

# Kinetic understanding of asymmetric amplification in amino-alcohol catalyzed organozinc additions

Jean-Claude Micheau,<sup>a,\*</sup> Thomas Buhse,<sup>b,\*</sup> Dominique Lavabre<sup>a</sup> and Jesús Rivera Islas<sup>b</sup>

<sup>a</sup>Laboratoire des IMRCP, UMR au CNRS No. 5623, Université Paul Sabatier, 118, Route de Narbonne, 31062 Toulouse Cedex, France

<sup>b</sup>Centro de Investigaciones Químicas, Universidad Autónoma del Estado de Morelos, Av. Universidad 1001, Col. Chamilpa, 62209 Cuernavaca, Morelos, Mexico

Received 9 October 2007; accepted 19 December 2007

**Abstract**—The dynamic features of Noyori's mechanism for the dimethylaminoisoborneol (DAIB) catalyzed alkylzinc addition to benzaldehyde have been investigated using the whole set of differential equations that describe the evolution of 19 species (starting products, intermediates, final compounds) involved in 36 coupled reversible or non-reversible processes. Using all the data available in the literature regarding the kinetic and thermodynamic parameters, the modeling confirms that the non-linear correlation between the enantiomeric excess of the chiral auxiliary ( $ee_{aux}$ ) and that of the product ( $ee_{prod}$ ) originates from the accumulation of the heterochiral alkylzinc amino alkoxide dimer (a reservoir effect). The variations of the enantiomeric excess of the product versus the benzaldehyde conversion are shown. Inhibition by the product can be understood by considering a reversible interaction between the alkoxide produced and the monomeric alkylzinc amino alkoxide catalyst. The effect of the order of the reactant addition on the  $ee_{prod}$  and the rate of reaction as observed with 1-piperidino-3,3-dimethyl-2-butanol (PDB) instead of DAIB can be simulated without changing the relative thermodynamic stabilities of the homo- and heterochiral dimers although at the expense of a slowing-down of their equilibration rates.  
© 2008 Elsevier Ltd. All rights reserved.

## 1. Introduction

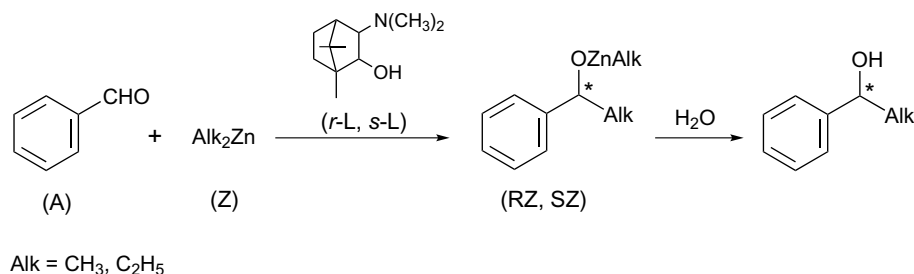
Non-linear effects in asymmetric synthesis (NLE) have attracted close attention in the search of efficient methods for enantioselective catalysis.<sup>1–3</sup> NLE stands for the condition in which the relation between the enantiomeric excess of the chiral auxiliary or catalyst ( $ee_{aux}$ ) and that of the product ( $ee_{prod}$ ) deviates from linearity so that the  $ee_{prod}$  can overcome the level of the  $ee_{aux}$  giving rise to the so-called asymmetric amplification. Due to such an increase in  $ee$ , NLE are not only relevant for new perspectives in synthetic organic chemistry but can also be regarded as a possible ingredient to rationalize the still puzzling origin of the enantiomeric homogeneity in Nature.<sup>4–6</sup>

Since the early discovery of NLE in the Sharpless epoxidation of geraniol,<sup>7,8</sup> various systems have been characterized that display these effects, where perhaps the most prominent cases belong to amino-alcohol catalyzed organozinc additions to aldehydes (Scheme 1).<sup>8–12</sup>

NLE are usually portrayed by spindle-shaped diagrams when plotting the  $ee_{prod}$  versus  $ee_{aux}$ , where asymmetric amplification is attributed to a positive deviation from a linear relationship between  $ee_{prod}$  and  $ee_{aux}$ . Generalized models to account for such observations are centered on the in situ formation of diastereomeric species either within or outside the enantioselective catalytic cycle. These can be represented by two extreme situations, the  $ML_n$  model on the one hand, or the reservoir model on the other.<sup>13</sup> The  $ML_n$  model describes the association of at least two chiral ligands with an involved metallic center to form equally stable homo- and heterochiral complexes but with different catalytic activities and stereoselectivities. On the other hand, the reservoir model considers the self-association between the chiral ligands leading to homo- and heterochiral dimers that differ in their thermodynamic properties and in their kinetics of association and dissociation, but do not display any catalytic activity.

The kinetics of NLE in amino-alcohol catalyzed dialkylzinc additions are still the subject of ongoing research.<sup>14–16</sup> More recently, additional observations have attracted further interest. First, it has been observed that the reaction rate and  $ee_{prod}$  can depend on the order in which the

\* Corresponding authors. Tel.: +33 561556275; fax: +33 561558155 (J.-C.M.); tel./fax: +52 7773297997 (T.B.); e-mail addresses: [micheau@chimie.ups-tlse.fr](mailto:micheau@chimie.ups-tlse.fr); [buhse@uaem.mx](mailto:buhse@uaem.mx); [dominique.lavabre@orange.fr](mailto:dominique.lavabre@orange.fr)



**Scheme 1.** (2*R*)- or (2*S*)-3-*exo*-(dimethylamino)-isoborneol (*r*-L or *s*-L) catalyzed addition of dialkylzinc to benzaldehyde yielding an optically active alcohol with a higher ee than that of the chiral auxiliary.

reactants are added to the reaction mixture.<sup>17</sup> Secondly, there is experimental evidence that the reaction mechanism includes some form of product inhibition,<sup>18</sup> which is of particular interest since product inhibition and product catalysis, as observed in the autocatalytic addition of diiso-propylzinc to pyrimidine carbaldehydes (the so-called Soai reaction),<sup>19,20</sup> are closely related phenomena.

The purpose of our paper is to analyze the dynamic behavior of the alkylzinc addition to benzaldehyde under consideration of the recent experimental observations and based on a kinetic model outlined by Noyori et al.<sup>21</sup> Following our previous attempts at a closer kinetic understanding of complex reaction mechanisms of this kind,<sup>22,23</sup> we took into account the full extent of coupled dynamics given by foremost elementary steps as well as the entire variety of species involved in the model to examine the whole dynamic features of the detailed Noyori mechanism. Hence, we avoided the use of a steady-state approximation as well as the consideration of a limited number of dimerization equilibria. Herein, we report a generalized kinetic understanding of asymmetric amplification that could be applied to a wider variety of asymmetric reaction systems of this type.

## 2. Results and discussion

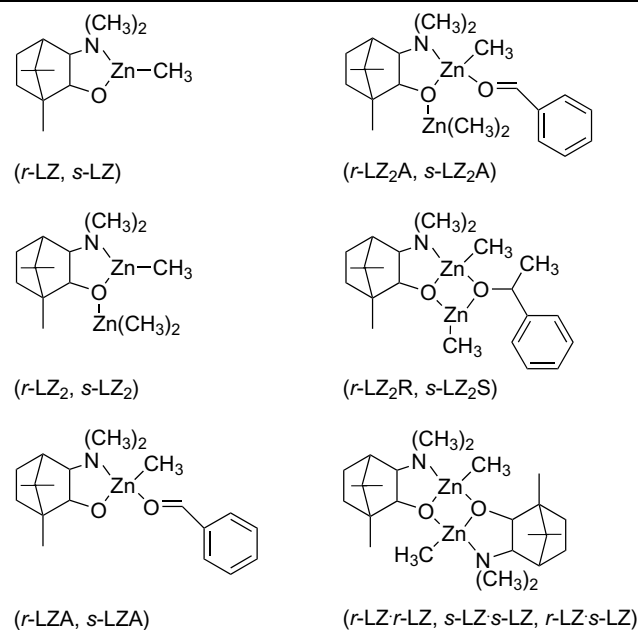
### 2.1. Kinetic modeling

We adopted the detailed kinetic model proposed by Noyori et al. for the addition of dimethylzinc (*Z*) to benzaldehyde (*A*) catalyzed by (2*R*)- and (2*S*)-3-*exo*-(dimethylamino)-isoborneol (*r*-L and *s*-L).<sup>†,21</sup> Table 1 outlines the compounds involved and their structural relationships.

Scheme 2 shows the model network that consists of 19 species and 36 steps, most of which are reversible. Each species is usually involved in several processes, as for instance the intermediate *r*-LZ (*s*-LZ) that takes part in six reversible reactions. The asymmetric reactions of the model were considered to proceed stereospecifically so that the unique link in the chemical processing between the species bearing either an (*S*)- or (*R*)-configuration is given by the forma-

<sup>†</sup>The proposal of this model scheme is essentially supported by NMR and crystallographic data as well as by ab initio molecular orbital studies.<sup>24,25</sup>

**Table 1.** Species and their acronyms used in the kinetic model of Scheme 2

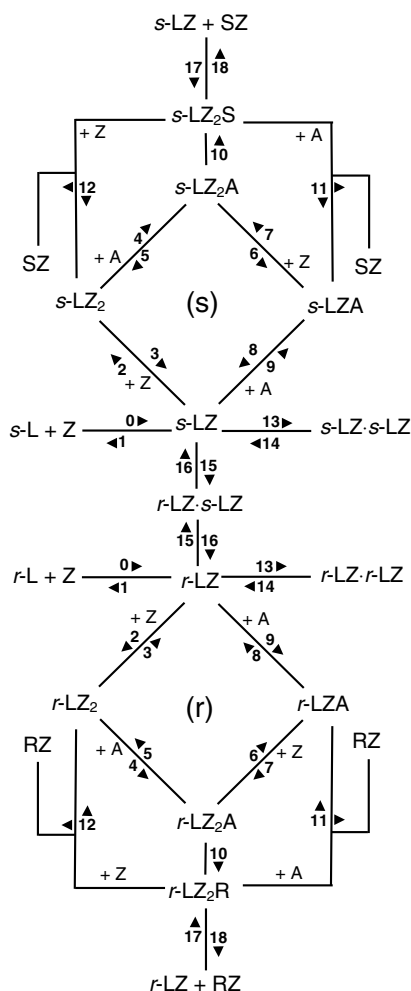


A, Z, *r*-L, *s*-L, RZ, and SZ are indicated in Scheme 1.

tion of the *r*-LZ·*s*-LZ dimer as the only mixed chiral compound (steps 15 and 16 in center of Scheme 2).

In the model, the reaction is initiated by the association of dialkylzinc (*Z*) to the chiral auxiliary (*r*-L or *s*-L). The resulting *r*-LZ or *s*-LZ species participate in the dimerization equilibria to yield *r*-LZ·*r*-LZ, *s*-LZ·*s*-LZ, or *r*-LZ·*s*-LZ dimers. These reversible processes are the crucial steps of the dynamics. As a result, the ee of the free *r*-LZ and *s*-LZ monomers that are not involved in the dimerization equilibria can increase because of the reversible formation of the optically inactive and catalytically inert *meso*-type *r*-LZ·*s*-LZ dimer. Therefore, amino-alcohol catalyzed dialkylzinc additions to benzaldehyde (Scheme 1) are suggested to be driven by a mechanism that can be related to the reservoir model.<sup>11</sup>

The species *r*-LZ and *s*-LZ also participate in one of the two stereospecific catalytic cycles (*r*) and (*s*) that involve several intermediates. The aldehyde (*A*) as well as the dialkylzinc (*Z*) react with *r*-LZ<sub>2</sub>R (*s*-LZ<sub>2</sub>S) to yield the reaction

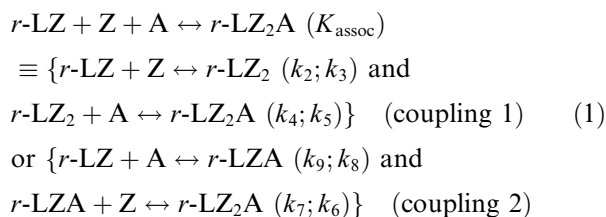


**Scheme 2.** Kinetic scheme adopted from Noyori et al.<sup>21</sup> (s) and (r) indicate the two enantioselective catalytic cycles for the formation of *S* and *R* products, respectively. For instance,  $r\text{-L} + \text{Z} \xrightleftharpoons[k_1]{k_0} r\text{-LZ}$  indicates the reversible formation of *r*-LZ:  $r\text{-L} + \text{Z} \leftrightarrow r\text{-LZ}$  ( $k_0$ ;  $k_1$ ).

products RZ (SZ) by which the catalytic intermediates *r*-LZA (*s*-LZA) and *r*-LZ<sub>2</sub> (*s*-LZ<sub>2</sub>) are recycled (steps 11 and 12, respectively). Due to the mirror-image symmetry, the processing for the *R* and *S* species essentially occurs with the same rate constants.

For the numerical simulations, Scheme 2 has been translated into a system of differential equations (see Section 4). Here, we have used rate parameter values that were partially issued from the literature data as given in Table 2. The remaining values  $k_0$ ,  $k_1$ ,  $k_{11}$  and  $k_{12}$  were to be assumed within a realistic order of magnitude and  $k_2$  to  $k_9$  were chosen sufficiently rapid and in agreement with the association constant  $K_{\text{assoc}}$  (see legend of Fig. 1).

The association constant  $K_{\text{assoc}} = 20 \text{ M}^{-2}$ , as given by Noyori et al.<sup>21</sup> merits a closer inspection. Taking into account its unit ( $\text{M}^{-2}$ ),  $K_{\text{assoc}}$  is likely related to an overall process  $r\text{-LZ}$  (or  $s\text{-LZ}$ ) + Z + A  $\leftrightarrow$   $r\text{-LZ}_2\text{A}$  (or  $s\text{-LZ}_2\text{A}$ ) resulting from the combination of two elementary processes imbedded in the stereospecific catalytic cycles (*r*) and (*s*). Considering the following equivalence, for instance, for the catalytic cycle (*r*)



$K_{\text{assoc}}$  can be transformed into a set of coupled equilibria giving rise to  $K_{\text{assoc}} = k_2k_4/k_3k_5 = k_7k_9/k_6k_8$ .

## 2.2. Time-evolution of the amino-alcohol catalyzed organozinc addition to benzaldehyde

The major benefit of performing numerical simulations based on the mechanism of Scheme 2 is to gain access to the time-evolution of the main species and the reaction intermediates involved.

**2.2.1. Evolution of the major species.** Figure 1 shows the time-evolution of the major species as a result of a typical simulation of Scheme 2.

Since Z is involved in more reactions, it is more consumed than A. The strong asymmetric amplification, which occurs during the carbinol synthesis with an ee exceeding 65% from an  $\text{ee}_{\text{aux}} < 6\%$ , is also shown. Under stoichiometric

**Table 2.** Parameters used for kinetic modeling derived from the literature (Ref. 21)

	Experimental value	Relation to Scheme 2	Parameter values used in the model
Thermodynamic homodimer dissociation constant	$K_{\text{RR}} = K_{\text{SS}} = 3 \times 10^{-2} \text{ M}$	$K_{\text{RR}} = K_{\text{SS}} = k_{14}/k_{13}$	$k_{14} = 3 \text{ s}^{-1}$ $k_{13} = 100 \text{ M}^{-1} \text{ s}^{-1\text{a}}$
Thermodynamic heterodimer dissociation constant	$K_{\text{RS}} = 10^{-5} \text{ M}$	$K_{\text{RS}} = k_{16}/k_{15}$	$k_{15} = 1.7 \times 10^4 \text{ M}^{-1} \text{ s}^{-1\text{b}}$
Kinetic rate constant of heterodimer dissociation	$k = 0.17 \text{ s}^{-1}$	$k_{16}$	$k_{16} = 0.17 \text{ s}^{-1\text{c}}$
Kinetic rate constant of alkyl migration	$k = 4.2 \times 10^{-3} \text{ s}^{-1}$	$k_{10}$	$k_{10} = 4.2 \times 10^{-3} \text{ s}^{-1\text{c}}$
Catalyst/reactant/substrate association constant	$K_{\text{assoc}} = 20 \text{ M}^{-2}$	$K_{\text{assoc}} = k_2k_4/k_3k_5 = k_7k_9/k_6k_8$	Variable values of $k_2$ to $k_9^{\text{d}}$

<sup>a</sup> Arbitrarily chosen, consistent with  $K_{\text{RR}} = K_{\text{SS}} = 3 \times 10^{-2} \text{ M}$ .

<sup>b</sup> Fulfilling  $K_{\text{RS}} = 10^{-5} \text{ M}$ , taking into account that  $k_{16} = 0.17 \text{ s}^{-1}$ .

<sup>c</sup> Directly taken from Ref. 21.

<sup>d</sup> Obeying  $K_{\text{assoc}} = 20 \text{ M}^{-2}$ .

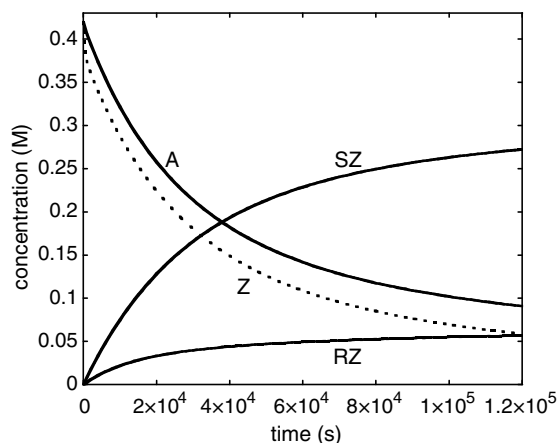


**Figure 1.** Simulated time-evolution of the major species during the addition of dimethylzinc (Z) to benzaldehyde (A) giving rise to the carbinol derivatives RZ and SZ ( $ee_{\text{prod}} = 66.7\%$ ). The following initial conditions and parameters were used for Scheme 2:  $[A]_0 = [Z]_0 = 0.42 \text{ M}$ ,  $[r\text{-L}]_0 = 0.016 \text{ M}$ ,  $[s\text{-L}]_0 = 0.018 \text{ M}$ ; (absolute  $ee_{\text{aux}} = 5.9\%$ );  $k_0 = 1000 \text{ M}^{-1} \text{ s}^{-1}$ ,  $k_1 = 100 \text{ s}^{-1}$ ,  $k_2 = k_9 = 4.5 \times 10^5 \text{ M}^{-1} \text{ s}^{-1}$ ,  $k_3 = k_8 = 10^7 \text{ s}^{-1}$ ,  $k_4 = k_7 = 4.5 \times 10^7 \text{ M}^{-1} \text{ s}^{-1}$ ,  $k_5 = k_6 = 10^5 \text{ s}^{-1}$ ,  $k_{11} = k_{12} = 100 \text{ M}^{-1} \text{ s}^{-1}$ ,  $k_{17} = k_{18} = 0$ ; other parameters were as given in Table 2.

$[A]/[Z]$  conditions, the reaction slows down as the global reaction—discounting the intermediates—could be resumed as  $A + Z \rightarrow \text{RZ}$  and  $\text{SZ}$ .

**2.2.2. Mean concentrations of the intermediates.** Table 3 gives the orders of magnitude of the mean concentrations of all the  $r\text{-L}$  and  $s\text{-L}$  containing intermediates during the course of the reaction. For the sake of clarity, the individual evolution of each intermediate is not shown. The principle intermediate is the heterochiral dimer  $r\text{-LZ}\cdot s\text{-LZ}$  with a mean concentration of  $10^{-2} \text{ M}$ . This comparatively high concentration causes the asymmetric amplification by the reservoir effect. The occurrence of the asymmetric amplification is revealed by the relative amounts of each catalytic complex.

During the course of the reaction, all chiral intermediates, such as  $r\text{-L}$ ,  $r\text{-LZ}$ ,  $r\text{-LZ}_2$ ,  $r\text{-LZA}$ ,  $r\text{-LZ}_2\text{A}$ , and also  $r\text{-LZ}_2\text{R}$  (respectively,  $s\text{-L}$ ,  $s\text{-LZ}$ ,  $s\text{-LZ}_2$ ,  $s\text{-LZA}$ ,  $s\text{-LZ}_2\text{A}$ , and also  $s\text{-LZ}_2\text{S}$ ) exhibit the same enantiomeric ratio,  $er = r\text{-L}/s\text{-L} = r\text{-LZ}/s\text{-LZ} = r\text{-LZ}_2/s\text{-LZ}_2 = r\text{-LZ}_2\text{A}/s\text{-LZ}_2\text{A}$ . This effect is due to the rapidly established equilibria of all the reversible processes involved within the catalytic cycles. The enantiomeric ratio  $er$  is deduced from the mass action law applied to all coupled equilibria. Its evolution can be understood by the transient storage of  $r\text{-L}$  and  $s\text{-L}$  into the heterochiral dimer  $r\text{-LZ}\cdot s\text{-LZ}$ . When A and Z are equimolar, Z is exhausted at the end of the reaction. As a consequence, the intermediates  $r\text{-LZ}$  and  $s\text{-LZ}$  are involved in the reverse processes  $r\text{-LZ} \rightarrow r\text{-L} + \text{Z}$  and  $s\text{-LZ} \rightarrow s\text{-L} + \text{Z}$  ( $k_1$ ) to replenish the Z depletion. Since all equilibria are coupled, the heterochiral dimer compensates for the  $r\text{-LZ}$  ( $s\text{-LZ}$ ) consumption by dissociation according to  $r\text{-LZ}\cdot s\text{-LZ} \rightarrow r\text{-LZ} + s\text{-LZ}$  ( $k_{16}$ ). The release of a racemic mixture of  $r\text{-LZ}$  and  $s\text{-LZ}$  into the reaction medium triggers

a rapid decrease in either the enantiomeric ratio or the enantiomeric excess of all the intermediates, as shown for high aldehyde conversion.

**2.2.3. Evolution of the enantiomeric excess of the carbinol products ( $ee_{\text{prod}}$ ).** Figure 2 shows that the evolution of the enantiomeric excess for the irreversibly produced RZ and SZ differs from that of the intermediates. This difference can be rationalized by considering that on the one hand, these products accumulate, but on the other hand, they are produced instantaneously with the same enantiomeric excess as the intermediates. When the enantioselectivity of the intermediates rises, the  $ee$  of RZ and SZ also increases but more gradually in a delayed manner. A small quantity of incoming higher  $ee$  of RZ and SZ is mixed with a larger quantity of lower  $ee$ . On the other hand, at high aldehyde conversion, the  $ee$  of the intermediates decreases and a small quantity of incoming lower  $ee$  of RZ and SZ is now mixed with a larger quantity of a higher one. As a result, the  $ee$  of the RZ and SZ products levels out and even slowly decreases.

Most of the spindle-shaped representations of NLE by plotting  $ee_{\text{prod}}$  versus  $ee_{\text{aux}}$ , as they are found in the literature,<sup>2,13,16,17</sup> serve to visualize the amplification effect as a function of variations in the initial conditions. To obtain a tractable algebraic expression of  $ee_{\text{prod}}$  versus  $ee_{\text{aux}}$ , steady-state conditions, rapid equilibria, and first-order kinetics are usually assumed. In these cases, no information about the variation of the  $ee_{\text{prod}}$  versus conversion of the aldehyde is obtained. In contrast, the approach presented in this paper allows the tracking of the complete evolution of all variables of the reaction from 0% to 100% conversion. Figure 3 shows the asymmetric amplification on the final product expressed by a simulation of Scheme 2.

Changes in the initial concentrations of the reactants and the chiral auxiliary have a considerable influence on the resulting  $ee$  of the reaction products. As expected, an increase of the chiral auxiliary concentration leads to a stronger pronounced asymmetric amplification, as it can be seen by comparing the curves (3) and (4) in Figure 3.<sup>‡</sup> Curves (4) and (2) show the effect of an  $[A]_0$  increase and curves (5) and (3) the effect of a  $[Z]_0$  increase. In both the cases, the asymmetric amplification is reduced by increasing the reactant concentration.

### 2.3. Factors influencing the dynamics

**2.3.1. Reactant concentration.** Figure 4 shows that the changes in the concentrations of A and Z influence the establishment of the dimerization equilibria, especially that of the heterodimer  $r\text{-LZ}\cdot s\text{-LZ}$ . A higher heterochiral dimer concentration is equivalent to a stronger reservoir effect giving rise to higher  $ee_{\text{prod}}$ .

<sup>‡</sup> Additional simulations have shown that Scheme 2 can reproduce well the further detailed effect of the chiral auxiliary concentration on the resulting  $ee_{\text{prod}}$  as reported by Kitamura et al.<sup>24</sup>

**Table 3.** Average concentration level of intermediates in the *r*-L ( $x=r$ ) and *s*-L ( $x=s$ ) catalyzed the addition of dimethylzinc (Z) to benzaldehyde (A)

Concentration (M)	<i>r</i> -LZ· <i>s</i> -LZ	<i>x</i> -LZ	<i>x</i> -LZ <sub>2</sub>	<i>x</i> -LZ <sub>2</sub> A	<i>x</i> -LZA	<i>x</i> -LZ· <i>x</i> -LZ	<i>x</i> -LZ <sub>2</sub> X
10 <sup>-2</sup>	■						
10 <sup>-3</sup>		<i>s</i>	<i>s</i>				
10 <sup>-4</sup>		<i>r</i>	<i>r</i>				
10 <sup>-5</sup>				<i>s</i>	<i>s</i>	<i>s</i>	
10 <sup>-6</sup>				<i>r</i>	<i>r</i>	<i>r</i>	
10 <sup>-7</sup>							<i>s</i>
10 <sup>-8</sup>							<i>r</i>

Same parameters as in Figure 1.

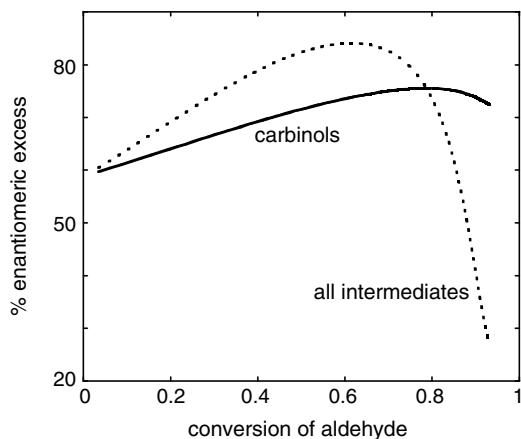


**Figure 2.** Evolution of the ee of all the intermediates and the ee of carbinols produced ( $ee_{\text{prod}}$ ) versus the aldehyde conversion (same parameters as in Fig. 1).

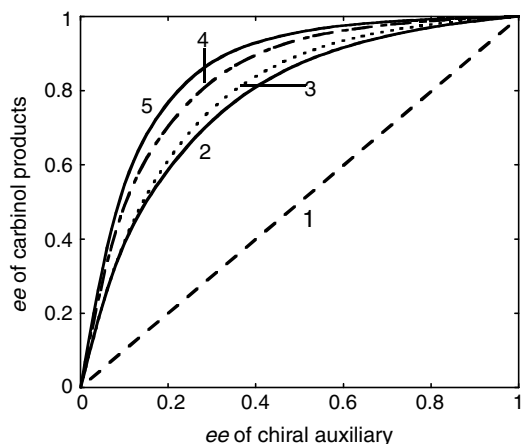


**Figure 3.** Visualization of the asymmetric amplification by simulation of Scheme 2 as a function of the enantiomeric excess of the chiral auxiliary (*r*-L and *s*-L). Curve 1 (no amplification) serves as a visual guide. The initial concentrations (in M) of [*r*-L + *s*-L]<sub>0</sub>, [A]<sub>0</sub>, and [Z]<sub>0</sub> were for curve (2) (solid line): 0.017, 0.84, and 1.68; curve (3) (dotted line): 0.0085, 0.42, and 1.68; curve (4) (dashed line): 0.017, 0.42, and 1.68; curve (5) (solid line): 0.0085, 0.42, and 0.84. Other parameters were as in Figure 1 and Table 2.

The comparison of the curves (1) and (3) of Figure 4 with the same  $[A]_0/[Z]_0 = 0.5$  initial stoichiometric ratio shows that at the onset of the reaction, that is, before arriving at the crossing point 'a', the heterodimer concentration is

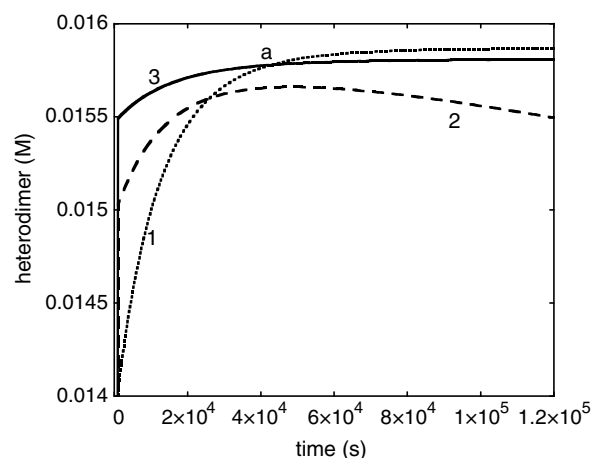


**Figure 4.** Influence of the aldehyde  $[A]_0$  and alkylzinc  $[Z]_0$  initial concentrations (in M) on the evolution of the heterochiral dimer *r*-LZ·*s*-LZ during the course of the reaction (simulation with the same parameter values of Fig. 1 and Table 2). Curve 1:  $[A]_0 = 0.42$ ;  $[Z]_0 = 0.84$ ; curve 2:  $[A]_0 = 0.42$ ;  $[Z]_0 = 0.42$ ; curve 3:  $[A]_0 = 0.21$ ;  $[Z]_0 = 0.42$ ; 'a' denotes the crossing point between curve 1 and curve 3 at >85% of conversion in the case of curve 1 and at about 70% of curve 3.

lower (weaker reservoir effect) when the reactants are more concentrated (curve 1). This effect is mainly due to an elevated storage in *s*-LZ<sub>2</sub>A (and *r*-LZ<sub>2</sub>A). At the crossing point 'a', the conversion of the aldehyde is rather high (>70%) in both the cases so that the  $ee_{\text{prod}}$  of both scenarios is mainly influenced by the early stage of the reaction. Since the reservoir effect for curve (1) is weaker than for curve (3), a lower  $ee_{\text{prod}}$  is expected. The simulations result in an  $ee_{\text{prod}}$  (1) = 58% while  $ee_{\text{prod}}$  (3) reaches a value as high as 76%. For curve (2), which is located between the curves (1) and (3) at the onset of the reaction, an intermediate ee value is expected ( $ee_{\text{prod}}$  (2) = 65.5%).

**2.3.2. Effect of  $ee_{\text{aux}}$  on the initial rate.** Due to the trapping of free *r*-LZ and *s*-LZ to form the heterodimer *r*-LZ·*s*-LZ, it is expected that the global rate of reaction reaches a minimum when the  $ee_{\text{aux}}$  approaches zero and arrives at a maximum if an enantiomerically pure chiral auxiliary is employed. To qualitatively illustrate this phenomenon, we have plotted in Figure 5 the variation of the initial rate versus the ee of the chiral auxiliary using the same graphical scales as in Ref. 11 (similar experimental results have been obtained by Buono et al.<sup>26</sup>).

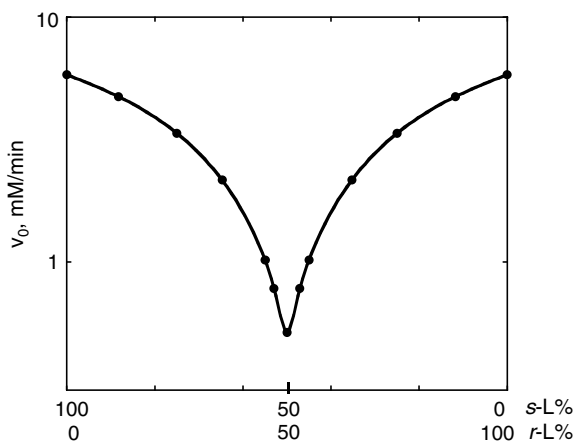


**Figure 5.** Initial rate of the amino-alcohol catalyzed organozinc addition to benzaldehyde as a function of the enantiomeric distribution of the chiral auxiliary. Simulation with parameter values of Figure 1 and Table 2 ( $[r-L]_0 + [s-L]_0 = 0.034$  M).

The ratio of the initial rates at  $ee_{\text{aux}} = 0\%$  versus  $ee_{\text{aux}} = 100\%$  is around  $0.5/5.8 \approx 1/10$ . This value is an estimate of the ratio of free *r*-LZ (*s*-LZ) with a maximum heterodimer ( $ee_{\text{aux}} = 0\%$ ) versus free *r*-LZ (*s*-LZ) without a heterodimer ( $ee_{\text{aux}} = 100\%$ ). When  $ee_{\text{aux}} = 0\%$ , the quantity of free *r*-LZ (*s*-LZ) depends, among other factors, on the degree of association of the heterodimerization equilibrium  $r\text{-LZ} + s\text{-LZ} \leftrightarrow r\text{-LZ}\cdot s\text{-LZ}$ . From the ratio of the rates, it is expected that in the present case only 10% of the auxiliary is free.

Corresponding experimental observations<sup>24</sup> on the effect of the catalyst and substrate concentrations on the initial rate are in good agreement with our model simulations.

**2.3.3. Rate constants.** Repeated simulations by increasing and decreasing the rate constants by several orders of magnitude, taking those given in Figure 1 and Table 2 as a reference, revealed several factors that can have a considerable influence on the overall rate of the reaction and on the asymmetric amplification. Possible effects have been evaluated by considering the  $ee_{\text{prod}}$  and the residual concentration of A at a given reaction time (usually at  $\approx 80\%$  conversion of the aldehyde). Reducing all the rates  $k_2$  to  $k_9$  within the catalytic cycle by three orders of magnitude while maintaining  $K_{\text{assoc}} = 20 \text{ M}^{-2}$  shows that both the reaction time and the enantioselectivity are increased. Also sensitive are  $k_{10}$ , which decreases the reaction time, and  $k_0$ , which increases the asymmetric amplification.

**Table 4.** Effect of a decrease in the rate of the dimerization equilibria on the onset of asymmetric amplification

$k_{13} (\text{M}^{-1} \text{s}^{-1})$	100	1	$10^{-2}$	$10^{-4}$	$10^{-6}$	$10^{-8}$
$[r\text{-LZ}\cdot s\text{-LZ}] (\text{M})$	$2.9 \times 10^{-3}$	$2.9 \times 10^{-3}$	$2.9 \times 10^{-3}$	$2.0 \times 10^{-3}$	$4.2 \times 10^{-5}$	$4.2 \times 10^{-7}$
$ee_{\text{prod}} (\%)$	77.6	77.4	68.1	28.1	25	25
% Conversion	92.9	86.4	86.8	92.6	94.7	94.8

$k_{13}$  to  $k_{16}$  have been reduced accordingly keeping the ratio  $K_{\text{RS}}/K_{\text{RR}} = (k_{14}k_{15})/(k_{13}k_{16}) = 3 \times 10^3$ . Other parameters are the same as in Figure 1 and Table 2, except  $([r-L]_0 + [s-L]_0) = 0.008$  M ( $ee_{\text{aux}} = 25\%$ ). Sufficient reaction time has been selected to arrive at more than 85% aldehyde conversion in the slowest case.

The case of variations in  $k_{13}$  to  $k_{16}$  (rates of dimerization and dimer-splitting) is particularly interesting. Here, we have reduced each individual rate constant maintaining the ratio of the thermodynamic dissociation constants,  $K_{\text{RS}}/K_{\text{RR}} = (k_{14}k_{15})/(k_{13}k_{16})$ , at its literature value of  $3 \times 10^3$ . Our results demonstrate that the onset of asymmetric amplification is not only of thermodynamic but it is also of kinetic origin. It is shown (right side of Table 4) that if the heterodimer *r*-LZ·*s*-LZ is not at an adequate concentration, the reservoir effect does not occur and, consequently, no asymmetric amplification takes place. For an efficient accumulation of the heterodimer within the reaction time, the heterodimerization equilibrium has to be sufficiently rapid.

## 2.4. Inhibition by the products

Rosner et al. reported that in amino-alcohol catalyzed dialkylzinc additions to benzaldehyde some form of product inhibition can occur.<sup>18</sup> Table 5a shows the transcription of the experimental data given by the authors that they have obtained by measuring the overall reaction rate after various repeated additions of fresh benzaldehyde during the course of the reaction.

**Table 5a.** Experimental data (from Ref. 18, Fig. 1) showing the half-time of benzaldehyde consumption and the reaction rate maximum after consecutive additions of fresh benzaldehyde ( $\sim 0.06$  M) to a reaction system initially consisting of  $\sim 0.014$  M (2*S*)-(–)-3-*exo*-(*N*-morpholino)-isoborneol and 1 M diethylzinc in toluene

Experimental run	$t_{1/2} (\text{s})$	Max rate ( $\text{mol L}^{-1} \text{s}^{-1}$ )
1	270	$2.1 \times 10^{-4}$
2	345	$1.7 \times 10^{-4}$
3	380	$1.1 \times 10^{-4}$
4	490	$0.9 \times 10^{-4}$

**Table 5b.** Approximate reproduction of the inhibition effect by model simulations of Scheme 2

Simulated run	$t_{1/2} (\text{s})$	Max rate ( $\text{mol L}^{-1} \text{s}^{-1}$ )
1	270	$2.4 \times 10^{-4}$
2	320	$2.0 \times 10^{-4}$
3	375	$1.8 \times 10^{-4}$
4	450	$1.5 \times 10^{-4}$

Each simulation was stopped after  $>95\%$  consumption of A and final concentrations of all species served as initial ones for the subsequent simulation except of A that was reinitialized at 0.06 M in each simulated run. To avoid the initial burst due to cycle establishment, the initial rates were taken after 50 s of reaction time. The same rate parameters were used as in Figure 1 and Table 2, except:  $k_{10} = 2.2 \times 10^{-2} \text{ s}^{-1}$ ,  $k_{17} = 5 \times 10^2 \text{ M}^{-1} \text{ s}^{-1}$ , and  $k_{18} = 5 \text{ s}^{-1}$ ,  $[s-L]_0 = 0.014$  M;  $[r-L]_0 = 0$ .

In the attempt to evaluate the present model for its capacity to reproduce such an effect, we have included in the model in Scheme 2 an interaction between the products RZ and SZ with the intermediate *r*-LZ or *s*-LZ, respectively (steps 17 and 18). By increasing  $k_{10}$  by less than one order of magnitude to reach approximately the experimentally observed reaction times and activating the *r*-LZ + RZ  $\leftrightarrow$  *r*-LZ<sub>2</sub>R and *s*-LZ + SZ  $\leftrightarrow$  *s*-LZ<sub>2</sub>S equilibria at a realistic value ( $k_{17}/k_{18} = 100 \text{ M}^{-1}$ ), it was possible to obtain a reasonable approximation of the experimental observations without changing any other parameter from Figure 1 and Table 2 (Table 5b).

### 2.5. Effect of the order at which the reactants are added

Regarding the dependency of the reaction rate and  $ee_{\text{prod}}$  on the order at which reactants are added to the reacting mixture as reported by Asakura et al.,<sup>17</sup> simulations with the present model (Scheme 2) could qualitatively reveal this effect by using appropriate rate parameters. We evaluated two cases. In procedure I, the simulation was started with the presence of *r*-L, *s*-L, and Z (absolute  $ee_{\text{aux}} = 5.9\%$ ), then, after *r*-LZ (*s*-LZ) equilibration, A has been added. In procedure II, *r*-L, *s*-L, A, and Z were initially present since there is no reaction between *r*-L (*s*-L) and A in our model. Hence, procedure II represents our normal simulation procedure.

It is apparent that a reactant order effect can only be observed if the equilibration of the processes involving *r*-L (and *s*-L) and Z is sufficiently slow, which is not the case for the rate parameters reported by Noyori et al. (Table 2).<sup>21</sup> Therefore, we attempted in the same way as in Section 2.4 to slow down adequately the dimerization equilibria by an arbitrary factor without changing the  $K_{\text{RR}}$  and  $K_{\text{RS}}$  equilibrium values. This factor had to be sufficiently high so that, for instance, the halftime of the *r*-LZ·*s*-LZ relaxation became of the same order of magnitude than that of the alkylation (*r*-LZ<sub>2</sub>A  $\rightarrow$  *r*-LZ<sub>2</sub>R or *s*-LZ<sub>2</sub>A  $\rightarrow$  *s*-LZ<sub>2</sub>R). These variations between parameters used to reproduce the addition order effect, with respect to those reported by Noyori et al.,<sup>21</sup> could be tentatively explained by the changes in the reaction conditions such as the use of PDB instead of DAIB, hexane instead of toluene and temperatures of  $-10 \text{ }^\circ\text{C}$  instead of  $40 \text{ }^\circ\text{C}$ , respectively. These differences may affect the corresponding rates of dimerization although the same reaction network is operating.

Figure 6 illustrates the different behavior observed for the evolution of A and  $ee_{\text{prod}}$  using either procedure I (pre-equilibration between Z and the chiral auxiliary) or procedure II (no pre-equilibration between Z and the chiral auxiliary).

The simulation clearly indicates that during procedure I, the reaction is slower but the  $ee_{\text{prod}}$  evolves to a higher value while procedure II gives rise to a more rapid process but to a lower value of  $ee_{\text{prod}}$ . Results of procedure II showing no or few asymmetric amplification are to be related to those reported on Table 4 for the slow equilibration assumption.

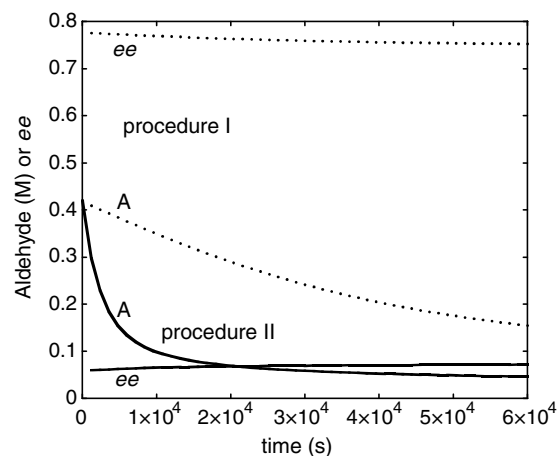


**Figure 6.** Effect of the order of reactant addition on the evolution of aldehyde A and  $ee_{\text{prod}}$  by simulation of Scheme 2. Procedure I: Pre-equilibration of the chiral auxiliary with alkylzinc and subsequent addition of A. Procedure II: Initial mixing of the chiral auxiliary, A and Z. Rate parameters as used in Figure 1 and Table 2 except  $k_{13} = 10^{-4} \text{ M}^{-1} \text{ s}^{-1}$ ,  $k_{14} = 3 \times 10^{-6} \text{ s}^{-1}$ ,  $k_{15} = 1.7 \times 10^{-2} \text{ M}^{-1} \text{ s}^{-1}$  and  $k_{16} = 1.7 \times 10^{-7} \text{ s}^{-1}$ .

### 3. Conclusion

Herein, we have outlined a general approach to analyze the dynamics that are at the origin of asymmetric amplification in amino-alcohol catalyzed dimethylzinc additions to benzaldehydes. The reaction network adopted from Noyori et al. proved to be versatile in accounting for the various experimental observations of these systems. Using experimentally determined rate parameters (when available), it was reiterated that asymmetric amplification originates from a reservoir effect, due to the formation of thermodynamically favored heterodimers. However, it was also demonstrated that the extent of asymmetric amplification does not only depend on the thermodynamic features of the system, but also on the velocities of various coupled reversible processes in the reaction network. Taking into account an interaction between the reaction products and the chiral auxiliary *r*-LZ (*s*-LZ), it was also possible to qualitatively reproduce an effect of product inhibition that is of further interest, because it can introduce kinetic non-linearity into such reaction systems that are already furnished with the capacity to show asymmetric amplification.

None of the simplifying assumptions frequently used in classical kinetics, such as initial rates, unique rate laws, rate limiting steps, or limited number of species and processes were applied. Supposing that realistic rate parameters were assumed, the time evolutions of all species are provided. This allows a global view over the various possible reaction regimes and the analysis of the whole variety of sometimes non-intuitive features of complex reaction systems like the amino-alcohol catalyzed organozinc addition to aromatic aldehydes.

### 4. Experimental

The given set of processes and rates of Table 6 were converted into the following set of differential equations:

**Table 6.** Processes and their rates used for the numerical simulations of Scheme 2

Process		Forward rate	Backward rate
$r\text{-L} + \text{Z} \leftrightarrow r\text{-LZ}$	$(k_0; k_1)$	$r_0 = k_0[r\text{-L}][\text{Z}]$	$r_1 = k_1[r\text{-LZ}]$
$s\text{-L} + \text{Z} \leftrightarrow s\text{-LZ}$	$(k_0; k_1)$	$r_{19} = k_0[s\text{-L}][\text{Z}]$	$r_{20} = k_1[s\text{-LZ}]$
$r\text{-LZ} + \text{Z} \leftrightarrow r\text{-LZ}_2$	$(k_2; k_3)$	$r_2 = k_2[r\text{-LZ}][\text{Z}]$	$r_3 = k_3[r\text{-LZ}_2]$
$s\text{-LZ} + \text{Z} \leftrightarrow s\text{-LZ}_2$	$(k_2; k_3)$	$r_{21} = k_2[s\text{-LZ}][\text{Z}]$	$r_{22} = k_3[s\text{-LZ}_2]$
$r\text{-LZ}_2 + \text{A} \leftrightarrow r\text{-LZ}_2\text{A}$	$(k_4; k_5)$	$r_4 = k_4[r\text{-LZ}_2][\text{A}]$	$r_5 = k_5[r\text{-LZ}_2\text{A}]$
$s\text{-LZ}_2 + \text{A} \leftrightarrow s\text{-LZ}_2\text{A}$	$(k_4; k_5)$	$r_{23} = k_4[s\text{-LZ}_2][\text{A}]$	$r_{24} = k_5[s\text{-LZ}_2\text{A}]$
$r\text{-LZA} + \text{Z} \leftrightarrow r\text{-LZ}_2\text{A}$	$(k_7; k_6)$	$r_7 = k_7[r\text{-LZA}][\text{Z}]$	$r_6 = k_6[r\text{-LZ}_2\text{A}]$
$s\text{-LZA} + \text{Z} \leftrightarrow s\text{-LZ}_2\text{A}$	$(k_7; k_6)$	$r_{26} = k_7[s\text{-LZA}][\text{Z}]$	$r_{25} = k_6[s\text{-LZ}_2\text{A}]$
$r\text{-LZ} + \text{A} \leftrightarrow r\text{-LZA}$	$(k_9; k_8)$	$r_9 = k_9[r\text{-LZ}][\text{A}]$	$r_8 = k_8[r\text{-LZA}]$
$s\text{-LZ} + \text{A} \leftrightarrow s\text{-LZA}$	$(k_9; k_8)$	$r_{28} = k_9[s\text{-LZ}][\text{A}]$	$r_{27} = k_8[s\text{-LZA}]$
$r\text{-LZ}_2\text{A} \rightarrow r\text{-LZ}_2\text{R}$	$(k_{10})$	$r_{10} = k_{10}[r\text{-LZ}_2\text{A}]$	—
$s\text{-LZ}_2\text{A} \rightarrow s\text{-LZ}_2\text{S}$	$(k_{10})$	$r_{29} = k_{10}[s\text{-LZ}_2\text{A}]$	—
$r\text{-LZ}_2\text{R} + \text{A} \rightarrow r\text{-LZA} + \text{RZ}$	$(k_{11})$	$r_{11} = k_{11}[r\text{-LZ}_2\text{R}][\text{A}]$	—
$s\text{-LZ}_2\text{S} + \text{A} \rightarrow s\text{-LZA} + \text{SZ}$	$(k_{11})$	$r_{30} = k_{11}[s\text{-LZ}_2\text{R}][\text{A}]$	—
$r\text{-LZ}_2\text{R} + \text{Z} \rightarrow r\text{-LZ}_2 + \text{RZ}$	$(k_{12})$	$r_{12} = k_{12}[r\text{-LZ}_2\text{R}][\text{Z}]$	—
$s\text{-LZ}_2\text{S} + \text{Z} \rightarrow s\text{-LZ}_2 + \text{SZ}$	$(k_{12})$	$r_{31} = k_{12}[s\text{-LZ}_2\text{S}][\text{Z}]$	—
$r\text{-LZ} + r\text{-LZ} \leftrightarrow r\text{-LZ} \cdot r\text{-LZ}$	$(k_{13}; k_{14})$	$r_{13} = k_{13}[r\text{-LZ}][r\text{-LZ}]$	$r_{14} = k_{14}[r\text{-LZ} \cdot r\text{-LZ}]$
$r\text{-LZ} + s\text{-LZ} \leftrightarrow r\text{-LZ} \cdot s\text{-LZ}$	$(k_{15}; k_{16})$	$r_{15} = k_{15}[r\text{-LZ}][s\text{-LZ}]$	$r_{16} = k_{16}[r\text{-LZ} \cdot s\text{-LZ}]$
$s\text{-LZ} + s\text{-LZ} \leftrightarrow s\text{-LZ} \cdot s\text{-LZ}$	$(k_{13}; k_{14})$	$r_{17} = k_{13}[s\text{-LZ}][s\text{-LZ}]$	$r_{18} = k_{14}[s\text{-LZ} \cdot s\text{-LZ}]$
$r\text{-LZ} + \text{RZ} \leftrightarrow r\text{-LZ}_2\text{R}$	$(k_{17}; k_{18})$	$r_{32} = k_{17}[r\text{-LZ}][\text{RZ}]$	$r_{33} = k_{18}[r\text{-LZ}_2\text{R}]$
$s\text{-LZ} + \text{SZ} \leftrightarrow s\text{-LZ}_2\text{S}$	$(k_{17}; k_{18})$	$r_{34} = k_{17}[s\text{-LZ}][\text{SZ}]$	$r_{35} = k_{18}[s\text{-LZ}_2\text{S}]$

$$d[r\text{-L}]/dt = -r_0 + r_1$$

$$d[\text{Z}]/dt = -r_0 + r_1 - r_2 + r_3 + r_6 - r_7 - r_{12} - r_{19} \\ + r_{20} - r_{21} + r_{22} + r_{25} - r_{26} - r_{31}$$

$$d[r\text{-LZ}]/dt = r_0 - r_1 - r_2 + r_3 + r_8 - r_9 - 2 \times r_{13} \\ + 2 \times r_{14} - r_{15} + r_{16} - r_{32} + r_{33}$$

$$d[r\text{-LZ}_2]/dt = r_2 - r_3 - r_4 + r_5 + r_{12}$$

$$d[\text{A}]/dt = -r_4 + r_5 + r_8 - r_9 - r_{11} - r_{23} + r_{24} + r_{27} \\ - r_{28} - r_{30}$$

$$d[r\text{-LZ}_2\text{A}]/dt = r_4 - r_5 - r_6 + r_7 - r_{10}$$

$$d[r\text{-LZA}]/dt = r_6 - r_7 - r_8 + r_9 + r_{11}$$

$$d[r\text{-LZ}_2\text{R}]/dt = r_{10} - r_{11} - r_{12} + r_{32} - r_{33}$$

$$d[\text{RZ}]/dt = r_{11} + r_{12} - r_{32} + r_{33}$$

$$d[r\text{-LZ} \cdot r\text{-LZ}]/dt = r_{13} - r_{14}$$

$$d[s\text{-LZ}]/dt = -r_{15} + r_{16} - 2 \times r_{17} + 2 \times r_{18} + r_{19} - r_{20} \\ - r_{21} + r_{22} + r_{27} - r_{28} - r_{34} + r_{35}$$

$$d[r\text{-LZ} \cdot s\text{-LZ}]/dt = r_{15} - r_{16}$$

$$d[s\text{-LZ} \cdot s\text{-LZ}]/dt = r_{17} - r_{18}$$

$$d[s\text{-L}]/dt = -r_{19} + r_{20}$$

$$d[s\text{-LZ}_2]/dt = r_{21} - r_{22} - r_{23} + r_{24} + r_{31}$$

$$d[s\text{-LZ}_2\text{A}]/dt = r_{23} - r_{24} - r_{25} + r_{26} - r_{29}$$

$$d[s\text{-LZA}]/dt = r_{25} - r_{26} - r_{27} + r_{28} + r_{30}$$

$$d[s\text{-LZ}_2\text{S}]/dt = r_{29} - r_{30} - r_{31} + r_{34} - r_{35}$$

$$d[\text{SZ}]/dt = r_{30} + r_{31} - r_{34} + r_{35}$$

Numerical simulations were carried out with the simulation-adjustment program SA 3.3 (non-commercial software, Laboratoire des IMRCP, Université Paul Sabatier, Toulouse, France). The general algorithm for the numerical integration of the differential equations was based on a

semi-implicit fourth-order Runge–Kutta method (SRK) with stepwise control for stiff ordinary differential equations. This numerical approach has been verified as sufficiently robust and reliable for the type of kinetic models treated in the present work.

### Acknowledgments

This work was funded by a bilateral Mexican–French cooperation project (CONACYT-CNRS Grant J110.515/2006). T.B. also acknowledges financial support from CONACYT Grant 52521.

### References

- Avalos, M.; Babiano, R.; Cintas, P.; Jiménez, J. L.; Palacios, J. C. *Tetrahedron: Asymmetry* **1997**, *8*, 2997–3017.
- Girard, C.; Kagan, H. B. *Angew. Chem., Int. Ed.* **1998**, *37*, 2922–2959.
- Kagan, H. B. *Synlett* **2001**, 888–899.
- Siegel, J. S. *Chirality* **1998**, *10*, 24–27.
- Avalos, M.; Babiano, R.; Cintas, P.; Jiménez, J. L.; Palacios, P. C. *Tetrahedron: Asymmetry* **2000**, *11*, 2845–2874.
- Sanders, P. G. H. *Int. J. Astrobiol.* **2005**, *4*, 49–61.
- Katsuki, K.; Sharpless, K. B. *J. Am. Chem. Soc.* **1980**, *102*, 5914–5976.
- Puchot, C.; Dunach, E.; Zhao, S.; Agami, C.; Kagan, H. B. *J. Am. Chem. Soc.* **1986**, *108*, 2353–2357.
- Oguni, N.; Matsuda, Y.; Kaneko, T. *J. Am. Chem. Soc.* **1988**, *110*, 7877–7878.
- Soai, K.; Niwa, S. *Chem. Rev.* **1992**, *92*, 833–856.
- Noyori, R.; Suga, S.; Oka, H.; Kitamura, M. *Chem. Record* **2001**, *1*, 85–100.
- Pu, L.; Yu, H. B. *Chem. Rev.* **2001**, *101*, 757–824.
- Guillaneux, D.; Zhao, S. H.; Samuel, O.; Rainford, D.; Kagan, H. B. *J. Am. Chem. Soc.* **1994**, *116*, 9430–9439.
- Gutman, I. *J. Serb. Chem. Soc.* **1999**, *64*, 447–452.

15. Gutman, I. *J. Serb. Chem. Soc.* **1999**, *64*, 681–684.
16. Blackmond, D. G. *Acc. Chem. Res.* **2000**, *33*, 402–411.
17. Asakura, K.; Yamamoto, T.; Inoue, S.; Osanai, S.; Kondopudi, D. K.; Yamaguchi, T. *Chem. Phys. Lett.* **2005**, *406*, 312–317.
18. Rosner, T.; Sears, P. J.; Nugent, W. A.; Blackmond, D. G. *Org. Lett.* **2000**, *2*, 2511–2513.
19. Soai, K.; Shibata, T.; Morioka, H.; Choji, K. *Nature* **1995**, *378*, 767–768.
20. Soai, K.; Kawasaki, T. *Chirality* **2006**, *18*, 469–478.
21. Kitamura, M.; Suga, S.; Oka, H.; Noyori, R. *J. Am. Chem. Soc.* **1998**, *120*, 9800–9809.
22. Rivera Islas, J.; Lavabre, D.; Grevy, J. M.; Hernández Lamonedá, R.; Rojas Cabrera, H.; Micheau, J. C.; Buhse, T. *Proc. Natl. Acad. Sci. U.S.A.* **2005**, *102*, 13743–13748.
23. Lavabre, D.; Micheau, J. C.; Rivera Islas, J.; Buhse, T. *J. Phys. Chem. A* **2007**, *111*, 281–286.
24. Kitamura, M.; Okada, S.; Suga, S.; Noyori, R. *J. Am. Chem. Soc.* **1989**, *111*, 4028–4036.
25. Yamakawa, M.; Noyori, R. *J. Am. Chem. Soc.* **1995**, *117*, 6327–6335.
26. Buono, F.; Walsh, P. J.; Blackmond, D. G. *J. Am. Chem. Soc.* **2002**, *124*, 13652–13653.